Effects of electric fields on the photodetachment cross section of the H^- ion near threshold

J. E. Stewart,* H. C. Bryant, P. G. Harris, and A. H. Mohagheghi
The University of New Mexico, Albuquerque, New Mexico 87131

J. B. Donahue, C. R. Quick, R. A. Reeder, and V. Yuan
Los Alamos National Laboratory, Los Alamos, New Mexico 87545

C. R. Hummer† and W. W. Smith
The University of Connecticut, Storrs, Connecticut 06268

Stanley Cohen‡
Drexel University, Philadelphia, Pennsylvania 19104
(Received 23 May 1988)

A study is presented of the photodetachment cross section of the H^- ion near the one-electron threshold in electric fields ranging from approximately 5×10^{-7} up to 2.4×10^{-4} a.u. The lowest-field data, nominally at zero field, are consistent with the Wigner threshold law for p-wave processes. At larger field values, photodetachment using σ-polarized laser light displays the expected lowering of apparent threshold and evidence of tunneling. Using π-polarized light, the same features are seen with the additional feature of oscillations superimposed on the cross section. Three complementary explanations are presented for the oscillations.

I. INTRODUCTION

The experiments described here are the most recent in a series exploring the H^- ion using the relativistic H^- beam at the Clinton P. Anderson Meson Physics Facility (commonly known as LAMPF for Los Alamos Meson Physics Facility) at the Los Alamos National Laboratory. The recent experiments have explored the behavior of the photodetachment cross section of the H^- ion in moderate electric fields. Much of this work is described in detail in a recent dissertation[1] and a preliminary report on part of the work has been already given.[2]

H^- provides a simple test of theoretical models of photodetachment from negative ions in electric fields. This paper describes experiments which tested three such models. The experimental technique was similar to earlier work at LAMPF.[3] The relativistic H^- beam at LAMPF intersected by a Nd:YAG (yttrium aluminum garnet) laser beam allows us to use the relativistic Doppler shift,

$$E_{\text{c.m.}}=\gamma E_{\text{lab}}(1+\beta\cos\alpha)\ , \tag{1}$$

to achieve a photon energy which is continuously tunable over a wide range in the rest frame of the target particles. $\beta=v/c$; $\gamma=1(1-\beta^2)^{1/2}$; α is the angle between laser beam and particle beam defined such that head-on is zero degrees; E_{lab} is the laboratory photon energy.

The Lorentz transformation for electric and magnetic fields (in SI units),

$$\begin{aligned}\mathbf{F}'_{\perp}&=\gamma(\mathbf{F}_{\perp}+\mathbf{v}\times\mathbf{B})\ ,\\ \mathbf{F}'_{\parallel}&=\mathbf{F}_{\parallel}\end{aligned} \tag{2}$$

allows us to impose a modest magnetic field in the laboratory frame which transforms to a substantial electrostatic field in the barycentric frame. We take the barycentric magnetic field interaction to be negligibly small in comparison to the electric field interaction.

The experiments described were mounted to explore the behavior of the photodetachment cross section of the H^- ion near the one-electron threshold in electric fields. In particular, we were motivated by a prediction of Reinhardt[4] that we would observe oscillations in the cross section in the case where the photons were polarized parallel to the imposed electric field. An earlier prediction of oscillations in the photodetachment cross section in electric fields was made by Fabrikant.[5] Recently, Wong *et al.*[6] formulated a general theory of photodetachment of a negative ion in an electric field, an approximation for which, presented by Rau and Wong,[7] dealt specifically with H^- photodetachment in moderate electric fields. Again, oscillations are predicted.

Two series of experiments were conducted. One looked at the effect of photodetaching the loosely bound (0.75 eV) second electron of the H^- ion in electric fields of as much as 1.3×10^6 V/cm using σ-polarized light. (σ polarization corresponds to the electric field of the light wave perpendicular to the applied electric field; π is parallel.) The second used a modified apparatus to look at the effect of π polarization, although with smaller fields, of the order of 0.2×10^6 V/cm.

The field-induced oscillations are a phenomenon roughly similar to that observed by a number of other workers looking at neutral atoms of Rb, Ba, and Na.[8] Theoretical explanations have been put forward by Harmin,[9] Luc-Koenig and Bachelier;[10] Rau;[11] Rau and Lu.[12] Blumberg *et al.*[13] have reported observation of oscillations in the S^- photodetachment cross section in the

presence of a *magnetic* field, where they presume the oscillations are due to the excitation of the detached electron to discrete cyclotron levels. An important difference between the negative ion and neutral atoms is that, in the former case, the photodetached electron sees, at long range, only a uniform electric field while, in the latter case, the electron moves in the combined Coulomb field of the core ion plus a uniform electric field.

An "electrostatic potential well" was built to look at the effects of a pure electric field on the cross section and an electron spectrometer was made to be used in conjunction with the potential well to detect electrons which, once photodetached, were "tagged" with an energy different from background electrons. Most of the data were taken using an older setup with one of two electromagnets supplying a motional electric field.

The potential-well–spectrometer combination was useful to prove that the ripple effect is due in fact to the electric field and not a combination of crossed electric and magnetic fields.

II. THEORY OF H^- PHOTODETACHMENT

We look at three situations for which we invoke different theories. These cases are photodetachment in zero field, in a dc electric field with a photon polarized perpendicular to the field (σ), and in a dc electric field with a photon polarized parallel to the field (π).

A. Zero field

At zero field, we expect the Wigner[14] threshold law to apply. Wigner found that the cross section is proportional to

$$(E-E_0)^{(2l+1)/2} , \tag{3}$$

where E is the energy of the photon and E_0 is the binding energy so that $(E-E_0)$ gives the kinetic energy of the detached electron. The angular momentum quantum number of the final two-body state is l. In the case of photodetachment of the H^- ion, $l=1$. We expect that the cross section will depend on $(E-E_0)^{3/2}$. The range of validity of the Wigner law must be determined by experiment.

Fano and Rau,[15] following Armstrong,[16] obtain a simple characterization of the H^- cross section over a wide energy range in atomic units,

$$\sigma=\frac{16\pi}{3(137)}\frac{E_0^{1/2}(E-E_0)^{3/2}}{E^3} . \tag{4}$$

B. π polarization

The impetus for the ripple experiment was the prediction by Reinhardt.[4] Reinhardt's approach is based on a time-dependent autocorrelation function Fourier transformed into the energy domain. Rau and Wong[6] have also predicted oscillations in the H^- cross section by considering a "frame transformation" of the system from spherical to cylindrical coordinates as the escaping electron leaves the short-range field dominated by the nucleus and moves to the far region dominated by the electrostatic field.

Several authors have explained electric field oscillations which appear in the photoionization cross section of *neutral* atoms. Harmin[9] modeled the data of Freeman *et al.*[8(b)] by considering two distinct regions: one where the Coulomb potential was dominant and the imposed electric field could be ignored and one where the electric field was dominant. Harmin's work provided a partial basis for Rau and Wong's predictions for negative ions. Luc-Koenig and Bachelier[10] proposed that the oscillations arise from cancellations of oscillator strengths of different Stark states due to symmetries between the wave functions and the light.

Rau[11] and Rau and Lu,[12] by considering neutral hydrogen in an electric field in parabolic coordinates, find that oscillations with equal spacing dependent on $F^{3/4}$ are present. These oscillations have, in fact, been observed in the photoionization spectrum of neutral hydrogen in an electric field.[17]

1. *Time-dependent autocorrelation approach*

Reinhardt[4] gives a specific theory for negative ions. The photodetachment cross section is given as (in Ref. 18)

$$\sigma(\omega)=2\pi\alpha a_0^2\omega\int \exp(i\omega t)\langle\phi(t)|\phi(0)\rangle dt . \tag{5}$$

Reinhardt assumed a Gaussian, p-wave initial state of the form

$$\phi(0)=2\sqrt{\alpha}\left[\frac{2a}{\pi}\right]^{3/4} z\exp[-a(x^2+y^2+z^2)] , \tag{6}$$

where $a=1/(8\rho^2)$ with ρ equal to the ionic radius.[19] A further assumption is that there is no final-state interaction between the detached electron and the neutron atom—a reasonable assumption in light of the fact that the multipole elements which describe the polarized atom decay rapidly with distance.

The final state $\phi(t)$ is given by

$$\phi(t)=\int d^3x' U(\mathbf{x},\mathbf{x}',t)\phi(0) , \tag{7}$$

where $U(\mathbf{x},\mathbf{x}'t)$ is the propagator for an electron in a dc electric field.

A substantial amount of algebra leads to the result

$$\sigma(\omega)=2\pi\alpha a_0^2\omega\int_{-\infty}^{\infty} e^{i\omega t}\left[\frac{4a-F^2t^2(1+iat)}{4a(1+iat)^{5/2}}\right] \times\exp\left[\frac{-F^2t^2}{24a}(3+iat)\right]dt , \tag{8}$$

which must now be numerically integrated.

2. *Frame-transformation approach*

Rau and Wong's[6] frame transformation is based on the work of Harmin[9] and Fano.[20] The problem is considered in spherical symmetry while the electron is close to the atom and essentially uninfluenced by the external field.

At some appropriate distance a transformation is made to the cylindrically symmetric wave function which describes the electron in an electrostatic field.

They write the cross section in an electric field as

$$\sigma^F(k)=\sigma^{F=0}(k)\int_{-\infty}^{k^2/2} d(q^2/2)|U_{ql}^F|^2 , \tag{9}$$

where $\sigma^{F=0}$ is the zero-field photodetachment cross section, Eq. (4). The initial energy $k^2/2$ is divided into energy in the z direction, along the field $q^2/2$ and transverse energy $(k^2-q^2)/2$.

U_{q1}^F gives the frame transformation between the spherical outgoing p electron wave function and the cylindrical wave function of the photoelectron in the field F_z,

$$U_{q1}^F=\begin{cases}(3\pi/k^3)^{1/2}(16F)^{1/6}\mathrm{Ai}'(-q^2/(2F)^{2/3}), & m=0\\ (3\pi/2k)^{1/2}(4/F)^{1/6}(1-q^2/k^2)^{1/2}\mathrm{Ai}(-q^2/(2F)^{2/3}), & m=\pm 1 .\end{cases} \tag{10}$$

Here Ai and Ai′ are the Airy function and its derivative.

Rau and Wong[6] point out three characteristics of the cross section. (1) Above threshold σ^F oscillates about $\sigma^{F=0}$ with an amplitude proportional to $F^{1/3}$. (2) σ^F is finite and positive at the zero-field threshold with a value proportional to F. (3) σ^F decreases rapidly and monotonically below threshold.

Additionally, they point out that the energies of maxima in the cross section are given by

$$E_n=\frac{(3\pi Fn)^{2/3}}{2} , \tag{11}$$

where $n=1,2,3,\ldots$.

3. Simple theory to find minima

Bryant *et al.*[2] use a simpler approach to predict the locations of minima in the cross section. Considering the final state of the electron simply to be that of an electron in a dc field, i.e., no final-state interaction, they show that the energy of a minimum in the cross section can be written as

$$E_s=-(eF)^{2/3}\left[\frac{\hbar^2}{2m}\right]^{1/3} a_s' , \tag{12}$$

where the a_s' are arguments of the Airy function at its extrema, $s=1,2,3\ldots$.[21] Then the photon energy required to make a transition to a minimum is E_s plus the electron affinity of H^- (0.7542 eV).[22]

By considering how the spreading wave function of the photodetached electron reflects off the barrier formed by the dc potential we can learn something about the coherence time of the process. If the time to travel to the barrier and back exceeds the coherence time of the photodetachment process, the reflected wave cannot interfere with that still emerging from the ion and we will see no ripples.

The time to travel to the classical turning point and back is given by

$$\tau=2\int_0^{E/eF}\frac{dx}{v}=\frac{\sqrt{8mE}}{eF} . \tag{13}$$

By observing the approximate energy where ripples fade away we have a measure of the coherence time and, through Heisenberg's uncertainty principle, a measure of experimental resolution.[23]

C. σ polarization

Without recourse to a detailed theory in the σ case, we can make some assumptions about the form of the cross section. When an electrostatic potential is superimposed on the binding potential of the ion, one side of the binding well will be depressed and tunneling becomes possible. We expect then to see an exponential decrease in the cross section below the zero-field threshold, with increasing electric field.

We define a classical threshold energy in an electric field as simply the energy needed to raise the electron up to the now depressed top of the well. But, as seen above, we must include the effect of tunneling.

As the kinetic energy of the ejected electron is increased, the details of the potential at threshold must become less and less important, so we expect the cross section to approach that of zero field.

A simple characterization of the potential is[24]

$$V(z)=-ezF-\frac{1}{2}\frac{\alpha e^2}{(r+r_p)^4} , \tag{14}$$

where α is the polarizability of the atom and $r_p=0.583a_0$.[25] We can use this to make a rough calculation of the classical threshold for comparison to the experimental result.

Rau and Wong's work[6] accommodates σ polarization as well as π. Equation 9 includes an $m=\pm 1$ result [see Eq. (10)], which is the σ polarization case. We became aware of their work too late to include a comprehensive analysis in this paper.

III. APPARATUS AND EXPERIMENTAL TECHNIQUE

A. Overview of experiment

The experimental setup is simple in concept. Figure 1 shows a large scale view of the apparatus as set up for one series of later experiments. Several pieces of equipment are shown which played no role in these experiments. These are the polarimeter, foil box, fluorescent well, and the Rydberg well.

Figure 2 shows the "vertical bender" detection scheme where the electric field in the interaction region was motional due to a laboratory magnet, and Fig. 3 shows the "electron spectrometer" scheme with a longitudinal

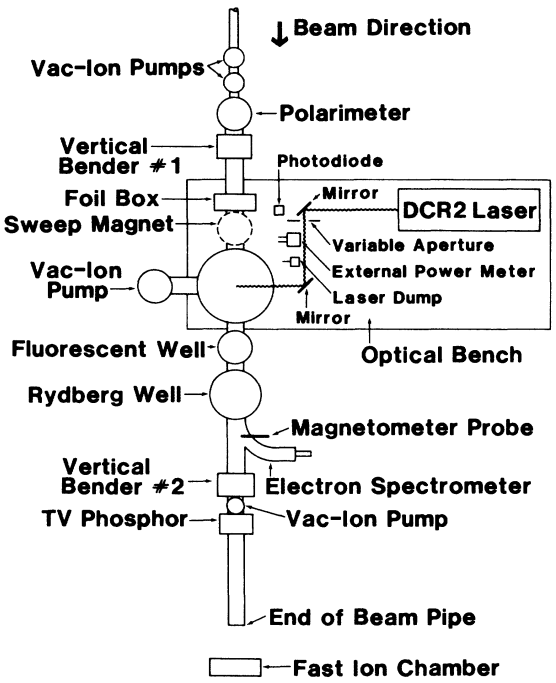

FIG. 1. Layout of later series of experiments.

electrostatic field in the interaction region. The vertical bender scheme was used in the earlier series and for the bulk of the later data. The electron spectrometer was used for a small portion of the later experiment. The changes to different detection schemes were small variations on the large scale setup, so Fig. 1 serves as a reasonable descriptor of all cases. The H^- beam entered the scattering chamber where it was intersected by a light beam at $\lambda = 1.06$ μm as seen in the laboratory from our Nd:YAG laser. The photon energy as seen by the H^- particles was dependent on the angles of intersection and is given by the Doppler formula, Eq. (1).

The products of the interaction were then detected downstream using one of two methods. In the first, the vertical bender scheme, the different charge states were magnetically separated and then the neutral products of the process were detected in a scintillator near the end of beam pipe (not shown in Fig. 1). In the second method,

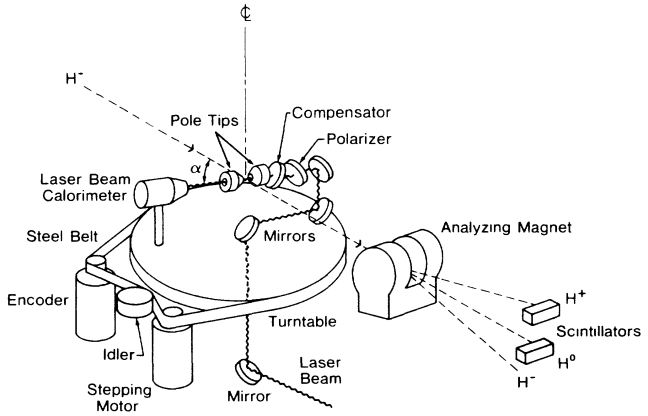

FIG. 2. Electromagnet in place.

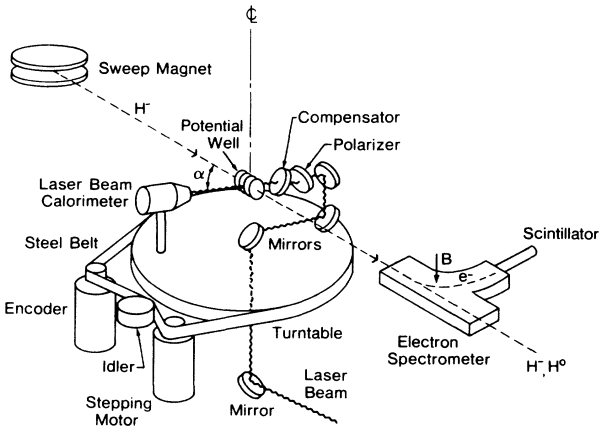

FIG. 3. Potential well in place.

which could be used only when no appreciable transverse magnetic field was present in the scattering chamber, electrons liberated in the photodetachment process were separated in an electron spectrometer with a momentum resolution of $\sim 1.5\%$ and detected by a small scintillator at the focal plane. In this case, we could distinguish electrons tagged in the electrostatic potential well with an energy difference of as little as 5 keV and so were able to discriminate against background electrons.

In past experiments we have used the laser in the Q-switched mode with a pulse width of ~ 8 ns and, due to jitter in the laser firing circuits comparable to the spacing of the H^- micropulses, the laser has been fired randomly into a macropulse giving a random overlap with any given micropulse. (The LAMPF H^- beam was delivered in macropulses of ~ 700 μs duration with a microstructure of pulses 0.25 ns wide, spaced 5 ns apart.) This technique gives high power densities and extremely low background counts. However, it requires relatively precise timing of detector circuits and may even saturate the micropulse so that essentially all the H^- are photodetached and the signal is no longer proportional to the photon current. In the later series we decided to try using the same laser in non-Q-switched mode. We simplified timing at the expense of additional background. The laser pulse was now ~ 100 μs, so, with roughly the same number of photons, our detector gates had to be open about 10^4 times as long as with the Q-switched mode. This change also eliminated our concern about saturating the H^- beam or the detector.

B. Methods to generate electric field

We used three methods to impose an electrostatic field on the interaction region in this experiment. Most of our field measurements were taken using one of two electromagnets.

In the earlier series the magnetic field imposed on the interaction region was normal to the laser-H^- plane so the motional electric field lay in the laser-H^- plane, perpendicular to the H^- beam. Because, near the Doppler free angle ($\cos\alpha = -\beta$), the laser beam appeared to the H^- to be near 90°, the laser was effectively σ polarized no matter how the laser was polarized in the laboratory frame.

In the later series most of our field measurements were taken using an electromagnet with holes through the pole tips to allow the laser beam to pass through, as shown in Fig. 4. This put the magnetic field in the same plane as the ion and laser beams. The magnet was mounted on the laser table, and thus it rotated with the laser beam. Because the electric field seen by the ion is dependent on the angle between the velocity vector and the magnetic field vector, the electric field changed as the angle of the laser changed.

The magnetic field being parallel to the laser beam gave a barycentric electric field normal to the laser-H^- plane; in this case, if the laser light was polarized normal to the laser-H^- plane, it would be pure π polarized and if it was polarized in the laser-H^- plane with the laser beam effectively at 90°, the light would be predominately σ polarized.

The third method of generating a field was to impose directly an electric field in the laboratory frame using a "potential well," as in Fig. 5. When using the potential well we detected and analyzed photodetached electrons that were tagged with a distinct energy depending on where in the well they were detached. An electron which existed in the beam in a free state before reaching the well passed through with no net change in energy. An electron which was freed through the photodetachment process between the center plates could emerge with an additional energy. The additional energy would then give a unique trajectory in the spectrometer.

IV. DATA AND ANALYSIS

The data discussed here are the results of a number of experiments spread over two years. Several different experimental setups under differing conditions were used. In the later series all of the data were taken at a primary beam energy of 500 MeV. We explored the H^- cross section using σ polarized light in large motional electric fields. In the later series we used two primary beam energies, 800 and 318 MeV and we looked at both σ and π polarization. We used the vertical bender detection scheme in the earlier series and for the later series 800 MeV runs. We used the electron spectrometer for the 318 MeV runs. Table I provides an overview of what was done when, and how it was done.

In our analysis we refer to the condition when the current in the magnet which provided the motional electric field was zero as "zero field," although at zero current there was still some residual magnetic field,

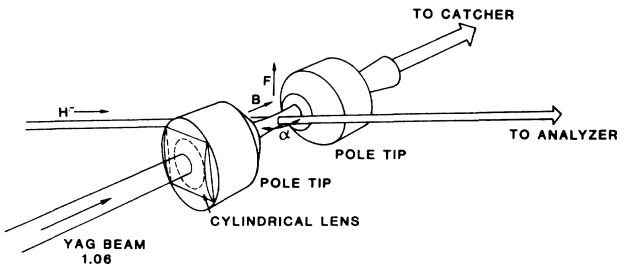

FIG. 4. Schematic of interaction region; vertical benders detection.

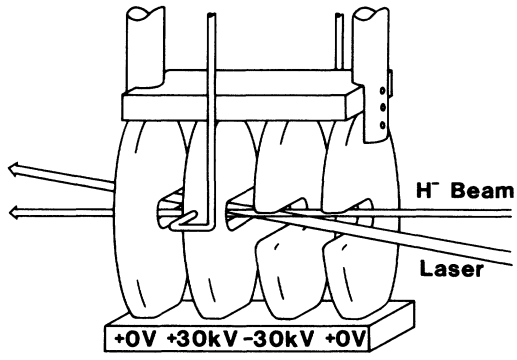

FIG. 5. Schematic of interaction region with potential well.

which in turn transformed into magnetic and electric fields in the rest frame of the ion. Typical residual fields varied from case to case, and will be given later.

The rest of the analysis will be divided into two groups with appropriate subdivisions. We will look at the earlier data first with consideration of the zero-field data and then of the field data which were all taken with σ polarization. Then the later data will be divided into three subtopics: zero field, σ-polarization field data, and finally π-polarization field data (the ripples). There are few later σ-polarization runs. They serve primarily to confirm the polarization dependence of the ripple phenomenon.

In the later experiments there was no on-line analysis of the data. Raw data were written to a file on the hard disc of the Micro-Vax and then were analyzed on a microcomputer using Lotus 1-2-3.[26]

The cross section was calculated using the formula

$$\sigma = GR\frac{\beta \sin\alpha}{IJ(1+\beta\cos\alpha)} , \tag{15}$$

where G is a geometric factor depending on the spatial and temporal overlap of the laser and particle beams, R is the rate of photodetachment, and J and I are the photon and ion currents, respectively.[27] Since we are unable to determine accurately the overlap, G becomes an arbitrary constant and we measure relative, not absolute, cross sections.

The zero-field data were analyzed to establish zero angle and the power law obeyed by the cross section above threshold. The data were first fit using a simplex routine[28] which fed its results into a covariant matrix calculation which computed the standard deviations of the fitted parameters.[29]

The function fitted to the zero-field data is a modification of Eq. (4),

$$\sigma = \frac{A(E-E_0)^P E_0^{1/2}}{E^3} + B . \tag{16}$$

Here are four parameters: A, an arbitrary amplitude; B, a background, which in theory should be zero; P, the exponent describing the behavior of the cross section above threshold; and E_0, the threshold.

Only the values of P and E_0 are of interest. Unfor-

TABLE I. Overview of experiments for (a) the earlier series and (b) the later series.

Beam energy	Experiment	Detection scheme
	(a)	
500 MeV	Zero field	Vertical benders
	Pure σ polarization	Vertical benders
	High motional electric fields	
	0–1.3 MV/cm	
	(b)	
800 MeV	Zero field	Vertical benders
	Pure σ or π polarization	Vertical benders
	Moderate motional electric fields	
	0–160 kV/cm	
318 MeV	Zero field	Electron spectrometer
	Pure π polarization	Electron spectrometer
	Low electrostatic fields	
	0–50 kV/cm	

tunately, we are unable to say anything about the absolute value of E_0. We use the fitted value of E_0 only as an approximate calibration. The value of P, however, is an important experimental result which we shall see approximately confirms the prediction made by the Wigner threshold law.

A. Earlier series zero-field data

The electromagnet used in the earlier series had a field at zero current of about 150 G. This transforms to 52 kV/cm (approximately 10^{-5} atomic units) at 500 MeV. This zero field which provided the basis for the earlier analysis, is of the order of the low field runs in the later runs.

The results from fits of zero-field data are summarized in the ideogram,[30] Fig. 6. All data files were cut off at approximately 0.805 eV and fit to Eq. (16). The files were then cut off closer and closer to threshold and fit again in order to determine the trend towards the power obeyed by the cross section at threshold. These data imply that the power law changes in the region between threshold and 0.8 eV, but we are reluctant to draw any conclusions from these data particularly in comparison to the later data. Recall that the Wigner prediction does not tell us how far above threshold the power of 1.5 should apply.

Several things are obvious from the data displayed in Fig. 6. A systematic error gives rise to the apparent grouping. These two groups correspond to data taken with the laser intersecting the H^- beam from different sides. An apparently anomalous data point has been dropped from this figure. It is included in Ref. 1. We see that one side gives consistently a lower power than the other. We have been unable to explain the discrepancy and must leave it to some unknown systematic error. We will see that this discrepancy does not exist in the later data.

B. Earlier series of σ-polarization field data

Data taken under σ polarization in the earlier series in various motional fields were parametrized by fitting with Eq. (16). These "Armstrong"[16] fits allow us to take a systematic look at the measurements.

Table II summarizes the results for all data from the earlier runs. As expected we see a lowering of threshold and an increase in exponent as electric field is increased. The "classical threshold" computed from Eq. (14) for each field value is given at the top of each column.

In Fig. 7, we see a series of data runs showing the progressive change in the cross section as the field is increased. Figure 8 illustrates the change in exponent and threshold as the field is increased.

C. Later series of zero-field data

Most of this zero-field data is not strictly taken at zero field, just as in the earlier series. The magnet used in the later series yielded a smaller transformed residual electric field, approximately 4.8 kV/cm, which would shift the classical photodetachment threshold downward by 0.5 mV. This shift is less than our experimental resolution but certainly large enough to be considered in the next generation of experiments.

All runs were cut off at the same maximum energy value for an initial look at the power law. With a maximum energy value of 0.80 eV the average fitted exponent

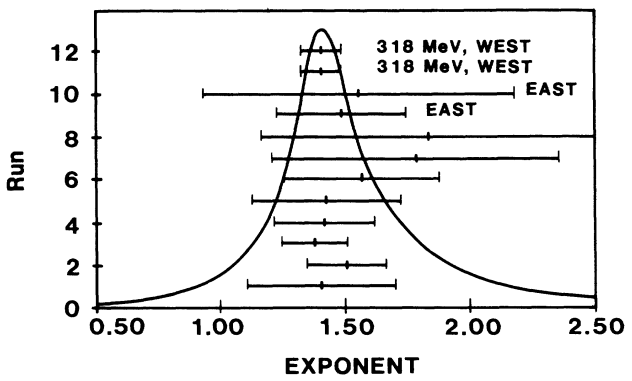

FIG. 6. Ideogram zero-field power-law fits for earlier series.

TABLE II. Average values of fitted parameters E_0 and P, with statistical errors in parentheses, from Eq. (16) for the earlier data. Data taken at various electric field values.

Electric field (MV/cm)	Zero field	0.35	0.68	1	1.18	1.32
Classical threshold (eV)	0.7542	0.7307	0.7144	0.7003	0.6927	0.6871
Fitted threshold, E_0	0.7618(5)[a]	0.7445(21)	0.6907(47)	0.666(12)	0.7044(71)	0.6509(37)
Fitted exponent, P	1.42(4)	2.08(14)	3.36(22)	4.4(6)	2.48(32)	3.45(13)

[a]This value should *not* be compared to the theoretical zero-field threshold for two reasons: the magnet giving rise to the motional electric field had some hysteresis and certain parameters used in the initial on-line analysis were incorrect. The errors in the parameters are approximately linear and should have little effect on the trends of fitted values shown here.

was 1.455(33). By successively truncating the data sets closer and closer to threshold we see a consistency that was not there in the earlier data. Figure 9 shows the results of this analysis. The plot labeled "all runs" includes the two truly zero-field runs taken at 318 MeV when the potential well was in place. These two runs yield the same values for the exponent: 1.41(8), consistent with the Wigner prediction of 1.5.

Table III summarizes the results of the zero-field fits which appear in Fig. 9. The ideogram in Fig. 10 shows the consistency between all of these runs.

D. Later series of σ-polarization field data

The eight data runs in this category serve primarily to verify the polarization dependence of the ripple phenomenon in the π data that we shall discuss below. The electric field strengths were not great enough to cause the obvious shifts in apparent threshold that can be seen in the earlier σ data.

These runs were fit with Eq. (16), but the results are not any more consistent than the earlier results. Figure 11 shows typical σ-polarization field data compared with π data.

E. Later series of π-polarization field data

Figure 12 shows curves generated with Reinhardt's[2] computer program, modified to model our experiment, superimposed on our π data. In what follows, we refer to the undulating character of cross sections as "ripples."

As mentioned earlier, the transformed electric field is not constant for these data. To find the electric field value at any point one can use the formula

$$F=\beta\gamma cB\sin\alpha\ ,$$

where

$$\alpha=\cos^{-1}\left[\frac{1}{\beta}\left[\frac{E}{\gamma E_L}-1\right]\right]\ . \tag{17}$$

The appropriate values for the constants are as follows: $\gamma=1.853$; $\beta=0.842$; $E_{\rm lab}=1.1648$ eV. The values for the

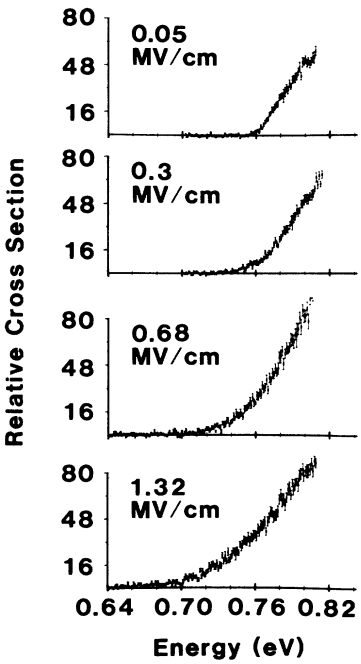

FIG. 7. Series of σ-polarization runs at different motional electric fields.

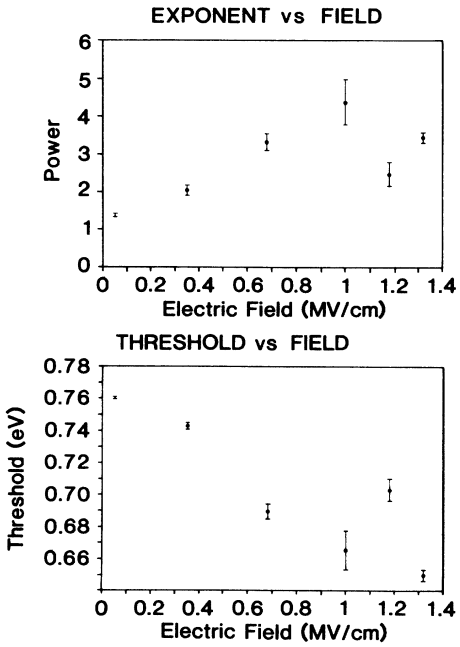

FIG. 8. Effect of electric field on exponent (power) and threshold.

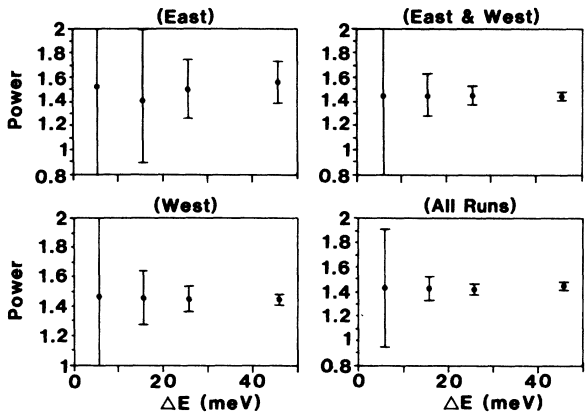

FIG. 9. Fits of power-law exponent for cross section for zero-field data taken in the later series. ΔE is the range of energies above threshold included in the data set. The maximum photon energy included is 0.80 eV.

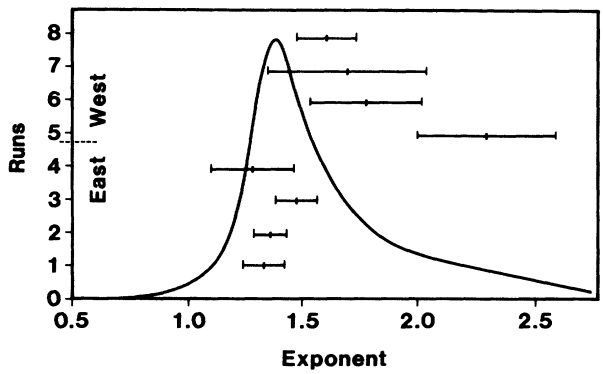

FIG. 10. Ideogram of later zero-field fits to the exponent in the power law for different runs.

magnetic field, B, appear in the appropriate figures.

Figure 13 shows the 143 kV/cm cross section from Fig. 12 now compared to the theory of Rau and Wong. In this case the data have been normalized to the theory at an arbitrary point which gives an absolute cross section.

The analysis of the ripple data was aimed at characterizing the location of the minima of the ripples. Since we assume the ripples are a modulation imposed on the zero-field cross section it seems reasonable to subtract the zero-field form from the ripple data to expose the ripple structure. This subtraction makes more apparent the exact location of the minima and maxima of the ripple structure. Figure 14 shows an example of the method.

The theory of Rau and Wong[6] leads us to expect that the oscillations should be symmetric about the zero-field curve but this does not appear to be the case in our data as it is presented here. This is at least partly an artifact of the method used to normalize the data with respect to the calculated zero-field curve. The data are normalized so that the maximum point is the same value as the maximum point of the zero-field curve which is chosen to be proportional to the maximum energy.

Once the subtraction was done we used visual interpolation of the plotted results to determine the location of minima. Additionally, we attempted to fit the minima individually with a Gaussian. The Gaussian shape is not a good descriptor of the shape of the ripples but it fit most of them easily, giving reasonable values for the minima with a useful error. About one-half the fits converged and they are generally in very good agreement with the eye.

Table IV also includes average values, labeled a_s' and n, as determined from the minima of the data. The a_s' values may be compared to the simple theory of Bryant *et al.*[2] where the energy of the minima are given by Eq. (12). The a_s' values were calculated using

$$a_s' = \frac{(E_{\min} - 0.7542 \text{ eV})}{-(eF)^{2/3}(\hbar^2/2m)^{1/3}} . \tag{18}$$

We include also a calculation of n from

$$n = \frac{2^{3/2}(E_{\min} - 0.7542 \text{ eV})^{3/2}}{3\pi F} , \tag{19}$$

based on Rau and Wong's statement, Eq. (11), for the maxima. The threshold value of 0.7542 eV must be converted to atomic units. We have assumed that the minima correspond to half integer values of n to make the comparison. The results are quite consistent with this premise.

Figure 15 plots the n values calculated from each data set versus energy. We have a consistent picture of a given oscillation associated with a particular value of a_s' or n; the energy location changes as the electric field is

TABLE III. Summary of fit to later zero-field data. Average fitted value of the parameter in Eq. (16). (Statistical errors in parentheses.)

	Data cut off			
	0.80 eV	0.78 eV	0.77 eV	0.76 eV
Laser on west side of H^- beam	1.45(3)	1.45(8)	1.46(18)	1.46(88)
Laser on east side of H^- beam	1.54(17)	1.50(24)	1.44(55)	
Laser on west side with truly zero field (taken at 318 MeV)		1.41(8)	1.42(17)	1.42(83)
Combined average	1.45(3)	1.43(6)	1.44(12)	1.44(60)

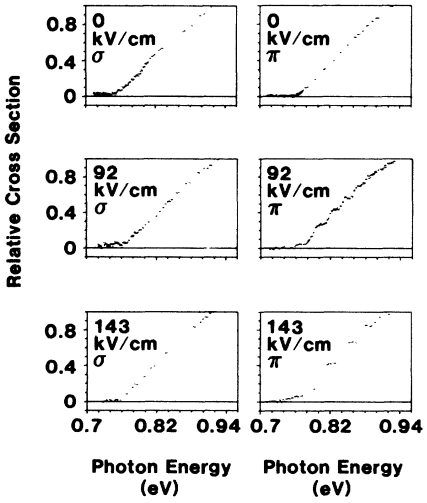

FIG. 11. Comparison of σ and π polarization at different electric fields.

changed but the order of the oscillation remains the same.

Rau and Wong have predicted that the amplitude of the oscillations about the zero-field curve will be proportional to $F^{1/3}$. We measured the peak-to-valley amplitude for the $n=\frac{1}{2}$ and $n=\frac{3}{2}$ minima and fitted the results with the equation

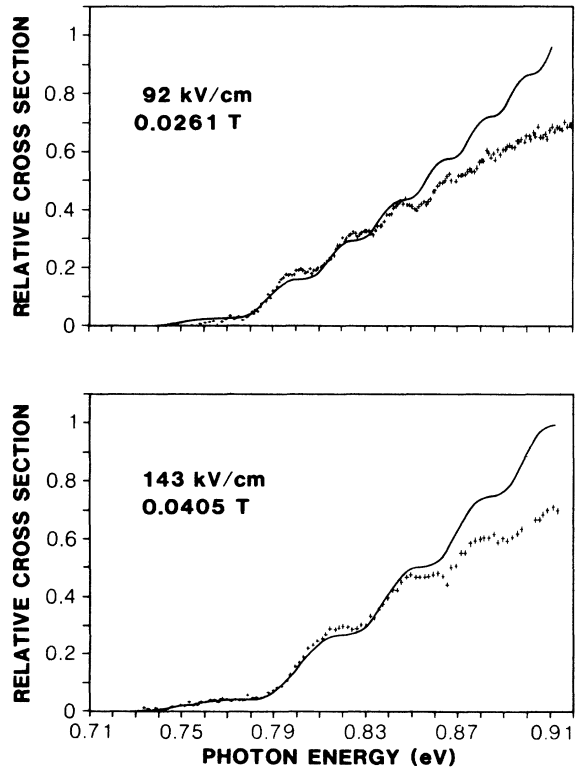

FIG. 12. Theoretical curves (solid lines) calculated from Reinhardt's theory compared to data (crosses). The laboratory frame value of the magnetic field producing the motional electric field is given.

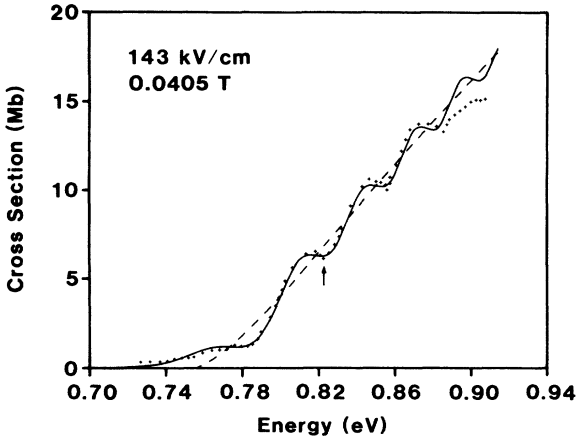

FIG. 13. Theoretical curve (solid line) calculated by Wong and Rau compared to data. The arrow marks the normalization point. The dashed line is the zero-field cross section.

$$A = A_0 \left[\frac{F}{F_0} \right]^P , \tag{20}$$

where A_0 and P are free parameters and F_0 was the lowest field value in the data set.

The data points were all given equal weights. The result of the fit is $P=0.340$ for $n=\frac{1}{2}$ and $P=0.333$ for $n=\frac{3}{2}$. The result is consistent with Rau and Wong's prediction.

There were three useful field runs taken with the potential well and the electron spectrometer. These runs give confirmation of the premise that the ripple effect is due solely to the electrostatic field. None of these runs is a particularly good example of the phenomenon. One has

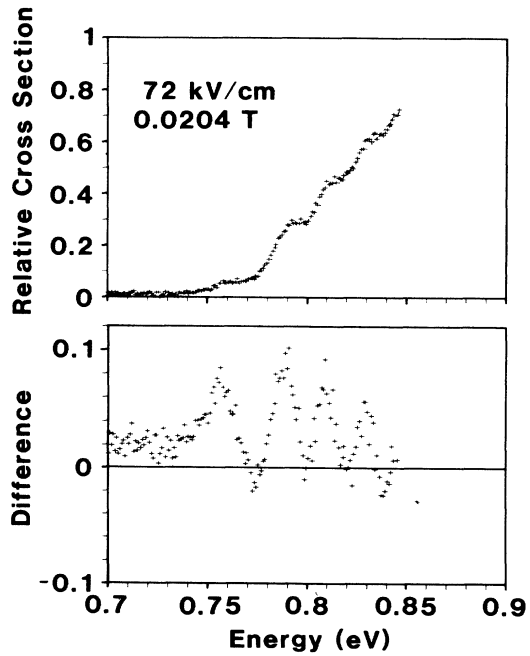

FIG. 14. Example of the subtraction method to extract ripple structure, as described in text.

TABLE IV. Average values for a_s' [treated as a parameter; using Eq. (18)] and for n [using Eq. (19)] for each order of oscillation. The true value of a_s' is defined as the values of the argument x of the Airy function Ai(x) at its extrema (Ref. 21, p. 478). (Statistical errors in parentheses.)

Average a_s'	True a_s'	Average n
−1.75(16)	−1.02	0.49(7)
−3.67(13)	−3.25	1.49(8)
−5.15(21)	−4.82	2.48(8)
−6.49(14)	−6.16	3.51(12)
−7.66(24)	−7.37	4.5(22)
−8.79(12)	−8.49	5.53(11)
−9.81(16)	−9.54	6.52(17)
−10.78(29)	−10.53	7.51(31)
−11.88	−11.48	8.7

only one distinguishable minimum. The other two have two minima.

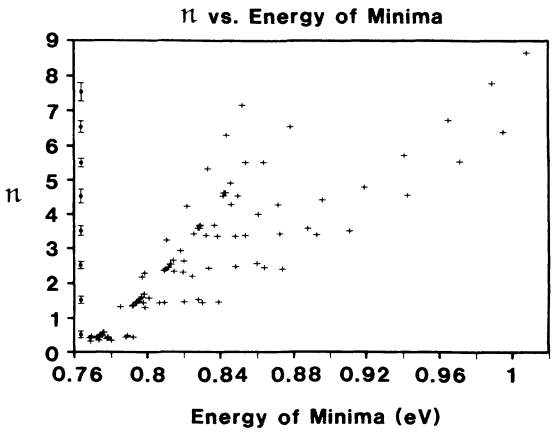

FIG. 15. The values of n plotted against energy for ripple minima for many different electric field values. The mean values of n are projected against the y axis.

V. CONCLUSIONS

We have examined the H^- photodetachment cross section in electric fields using both π- and σ-polarized laser light. With π-polarized light we have data taken with fields from 0 to 164 kV/cm. With σ-polarized light our data was taken at fields ranging from 52 kV/cm (the putative zero-field data from the earlier series) to 1.32 MV/cm.

In our analysis we compared the data with the Wigner threshold law which applies in the zero-field case. The zero-field data from the earlier series are consistent with a threshold power of 1.5. In the later series, although most of the data were taken with a small residual electric field of about 10^{-6} atomic units, we conclude that the data are consistent with the Wigner law at least as far as 46 meV above threshold. The two runs taken with no residual field yield a power law with exponent consistent with that predicted by Wigner.

The σ-polarization data give a qualitative confirmation of the expectations described earlier. The cross section is apparently exponential below the zero-field threshold, and it appears to follow the zero-field cross section well above the zero-field threshold.

The π-polarization data are consistent with all three of the theories described. The theory of Reinhardt does not conform well to the overall shape of the cross section above about 0.85 eV, although he has predicted the approximate location of minima well.

The theory of Rau and Wong, by describing the cross section in a field as a modulation on the zero-field cross section, does follow the general shape of the data as it begins to turn down at about 0.85 eV. Their specific prediction for the maxima of oscillations is in very good agreement with our data. We find the positions of minima to be well described by half integer values of n from Eq. (18) and, by inference, believe the maxima to be well described by integer values of n.

In a rather crude fashion we also confirm the prediction that the amplitude of the oscillations is proportional to $F^{1/3}$. For the first two cycles of oscillation we find the amplitudes to be proportional to $F^{0.34}$ and $F^{0.33}$, respectively.

We confirm two other qualitative statements by Rau and Wong. In an electric field the cross section is finite and positive at the zero-field threshold and it decreases rapidly and monotonically below threshold.

We emphasize the fact that our analysis of field data and the theories which describe them tell us nothing about the detailed structure of the H^- ion itself. The oscillatory structure observed is what one would see if a free electron suddenly appeared in a dc electric field. Reinhardt[4] assumes a generalized symmetric initial state and a final state of a free electron in an electrostatic field. We need only input the value of the zero-field threshold. Rau and Wong[6] include the zero-field H^- cross section only after the details of the process have been worked out, independently of the ion. Bryant *et al.*[2] use only the zero-field threshold energy as input for their prediction of minima.

In future experiments we will look for deviations from Rau and Wong's theory in the region just below and just above the zero-field threshold. It is here that the cross section should be most sensitive to the details of the H^- binding potential. We see no obvious deviations in our data but a very careful study with this objective in mind would give confirmation of the fine details of the theory. Complete tabulation of the data is available in Ref. 1.

ACKNOWLEDGMENTS

This work was done under the auspices of the U. S. Department of Energy in part by the Division of Chemical Sciences, Office of Basic Energy Sciences, Office of Energy Research (Contract No. DE-AS04-77ER03998) and in part by the U. S. Army Strategic Defense Command. We thank W. P. Reinhardt, A. R. P. Rau, and I. A. Sellin for their help and advice, and Carol Harvey Johnstone for her help with the earlier experiment.

*Present address: Western Washington University, Bellingham, WA 98225.
†Present address: Argonne National Lab, Argonne, IL 60439.
‡Present address: Cohen Mechanical Design, 719 Hedgrerow, Broomall, PA 19008.

[1]J. E. Stewart, Ph.D. dissertation, The University of New Mexico, Albuquerque, NM 87131. Available as Los Alamos National Laboratory Report No. LA-11152-77, UC-34, 1987.
[2]H. C. Bryant, A. Mohagheghi, J. E. Stewart, J. B. Donahue, C. R. Quick, R. A. Reeder, V. Yuan, C. R. Hummer, W. W. Smith, Stanley Cohen, R. P. Reinhardt, and L. Overman, Phys. Rev. Lett. **58**, 2412 (1987).
[3]H. C. Bryant, D. A. Clark, K. B. Butterfield, C. A. Frost, H. Sharifian, H. Tootoonchi, J. B. Donahue, P. A. M. Gram, M. E. Hamm, R. W. Hamm, J. C. Pratt, M. A. Yates, and W. W. Smith, Phys. Rev. A **27**, 2889 (1983).
[4]W. P. Reinhardt, in *Atomic Excitation and Recombination in External Fields,* edited by M. H. Nayfeh and C. W. Clark (Gordon and Breach, New York, 1985), p. 85.
[5]I. I. Fabrikant, Zh. Eksp. Teor. Fiz. **79**, 2070 (1980) [Sov. Phys.—JETP **52**, 1045 (1980)].
[6]H. Wong, A. R. P. Rau, and C. H. Greene, Phys. Rev. A **37** 2393 (1988).
[7]A. R. P. Rau and H. Wong, Phys. Rev. A **37**, 632 (1988).
[8]S. Feneuille, S. Liberman, J. Pinard, and A. Taleb, Phys. Rev. Lett. **42**, 1404 (1979); (b) R. R. Freeman, N. P. Economou, G. C. Bjorklund, and K. T. Lu, *ibid.* **41**, 1463 (1978); (c) M. G. Littman, M. M. Kash, and D. Kleppner, *ibid.* **41**, 103 (1978); (d) T. S. Luk, L. DiMauro, T. Bergeman, and H. Metcalf, *ibid.* **47**, 83 (1981); (e) W. Sandner, K. A. Safinya, and T. F. Gallagher, Phys. Rev. A **23**, 2448 (1981).
[9]D. A. Harmin, Phys. Rev. Lett. **49**, 128 (1982).
[10]E. Luc-Koening and A. Bachelier, Phys. Rev. Lett. **43**, 921 (1979).
[11]A. R. P. Rau, J. Phys. B **12**, L193 (1979).
[12]A. R. P. and K. T. Lu, Phys. Rev. A **21**, 1057 (1980).
[13]W. A. M. Blumberg, R. M. Jopson, and D. J. Larson, Phys. Rev. Lett. **40**, 1320 (1978).
[14]E. P. Wigner, Phys. Rev. **73**, 9, 1002 (1948).
[15]U. Fano and A. R. P. Rau, *Atomic Collisions and Spectra* (Academic, Orlando, 1986), Sec. 7.2.4.
[16]B. A. Armstrong, Phys. Rev. **131**, 1132 (1963).
[17]*Atomic Excitations and Recombination in External Fields,* edited by M. H. Nayfeh and C. W. Clark (Gordon and Breach, New York, 1985). See articles by M. H. Nayfeh *et al.*, p. 181, W. W. Smith *et al.*, p. 211, and H. Rottke *et al.*, p. 251.
[18]The matrix element has, in fact, been squared as expected, but is not explicitly displayed due to a mathematical trick which is exposed in E. J. Heller, J. Chem. Phys. **68**, 1066 (1978).
[19]L. Overman, Masters thesis, University of Pennsylvania, 1985.
[20]U. Fano, Phys. Rev. A **24**, 619 (1981).
[21]*Handbook of Mathematical Functions,* Natl. Bur. Stand. Appl. Math. Ser. No. 55, edited by M. Abramowitz and I. A. Stegun (U. S. GPO, Washington, D. C., 1964).
[22]C. L. Pekeris, Phys. Rev. **112**, 1649 (1958).
[23]A further exposition of this approach is given by H. C. Bryant, in Proceedings of Conference on Atomic Spectra and Collisions in External Fields II, Egham, Surrey, U. K., 1987, edited by K. T. Taylor M. H. Nayfeh, and C. W. Clark (unpublished).
[24]H. B. Delone, I. Yu. Kiyan, V. P. Krainov, and V. I. Tugushev, Opt. Spectrosk. **58**, 262, 1985 [Opt. Spectrosc. (USSR) **58**, 157 (1985)].
[25]L. I. Schiff, *Quantum Mechanics,* 3rd ed. (McGraw-Hill, New York, 1968), p. 265.
[26]Lotus 1-2-3, V. 2.0, Lotus Development Corp., Cambridge, MA (1985).
[27]H. C. Bryant, P. A. Lovoi, and G. G. Ohlsen, Phys. Rev. Lett. **27**, 1628 (1971).
[28]M. S. Caceci and W. P. Cacheris, Byte **9** (5), 340 (1984).
[29]D. Whitman, Computer code NONLIN, Baker Laboratory, Cornell University, 1982.
[30]An ideogram is a convenient method to examine the consistency of a set of data. The ordinate is an arbitrary run number. The abscissa is the value of the fitted parameter. Each point is displayed with the appropriate error bar. The curve is the sum of a Gaussian probability function calculated for each point. The area under each curve is $1/\sigma$ rather than $1/\sigma^2$ so that systematic errors are emphasized. Consistent data will show a singly peaked symmetric curve.